# Dancing synchronization in coupled spin-torque nano-oscillators

H. T. Wu [1,2] Lei Wang (王蕾) [1] Tai Min [1,*] and X. R. Wang [2,3,†]

[1]*Center for Spintronics and Quantum Systems, State Key Laboratory for Mechanical Behavior of Materials,*
*Xi'an Jiaotong University, 28 Xianning West Road, Xi'an, Shaanxi 710049, China*
[2]*Department of Physics, The Hong Kong University of Science and Technology,*
*Clear Water Bay, Kowloon, Hong Kong, China*
[3]*HKUST Shenzhen Research Institute, Shenzhen 518057, China*

We report a type of synchronization, termed *dancing synchronization*, between two spin-torque nano-oscillators (STNOs) coupled through spin waves. Different from the known synchronizations in which two STNOs are locked with various fixed relative phases, in this synchronized state two STNOs have the same frequency, but their relative phase varies periodically within the common period, resulting in a dynamic waving pattern. The amplitude of the oscillating relative phase depends on the coupling strength of two STNOs, as well as the driven currents. The dancing synchronization turns out to be universal and can exist in two nonlinear Van der Pol oscillators coupled both reactively and dissipatively. Our findings open the door for new functional STNO-based devices.

## I. INTRODUCTION

Synchronization is the coordination of different parts of a system working in harmony and is a ubiquitous phenomenon that has been observed in various branches of science ranging from physical systems to chemical and biological systems with gain and loss [1–5]. Together with other nonlinear effects and beyond, it increases the complexity of nature and organizes things at higher levels [6]. Synchronization was first discovered by Huygens in 1665 [7]. He found that two pendulum clocks hung side by side would soon swing with the same frequency and 180° out of phase regardless their initial conditions as long as their intrinsic frequencies were not too different from each other and their coupling strengths were not too weak. This completely out of phase synchronized motion is very robust against external disturbances. Since then, our understanding of synchronization has been greatly advanced.

Two coupled nonlinear oscillators in currently known synchronizations oscillate with the same frequency but can have different constant relative phases [1,7–9]. They are relatively simple and can be characterized by the frequency and their relative phase. For more exotic synchronizations, one needs to couple many nonlinear oscillators as a cluster or a network [10] that is commonly described by the Kuramoto model [9]. As summarized by Matheny and coworkers [11], the simplest synchronizations of many oscillators are ones in which all oscillators have the same phase or a few fixed relative phases. The relative phases of a synchronized oscillator network can even form a complicated static pattern. Sometimes, a network can fragment into several clusters, and motions of oscillators in each cluster are synchronized with their own static phase

pattern. In a word, the patterns of phase difference among oscillators in known synchronizations are static and do not change with time whether in two coupled oscillators or in an oscillator network.

Spin-torque nano-oscillators (STNOs) are important nonlinear oscillators in magnetics. STNOs [12,13] are self-sustained oscillations driven by current-generated spin-transfer torque (STT) [14,15]. Self-sustained oscillations are a well-known nonlinear phenomenon widely existing in systems with gain and loss [1,16,17]. STNOs are an active research topic in academia and industry because of their exotic applications in nanotechnology such as microwave generation at nanometer scale that is crucial for microwave-assisted recording [18,19]. Output power is an important issue in STNOs [20] because microwave power from a single STNO is of the order of picowatts due to its tiny size [21]. One promising way of increasing the output microwave power is through an in-phase synchronization of many STNOs [22,23]. Several STNOs can be coupled by static magnetic interaction [24–26]. This coupling is effective only when two STNOs are separated within a few nanometers, which limits the possible number of STNOs in synchronization. Coupling between STNOs through spin waves is order of magnitudes larger than that by static magnetic interaction [20,27–32]. Like other nonlinear systems, various aspects of coupled STNOs have been extensively studied, such as intrinsic mutual phase locking [22,33–35], STNOs due to the vortex state [36], and fractional synchronization [37]. The temperature [38] and external field [39] have been used to control the frequency, the linewidth of STNOs, and synchronization.

In this study, we report a type of synchronization of two STNOs coupled by spin waves. In this synchronization the relative phase of two oscillators varies periodically with time, instead of being constant. Such an exotic synchronization is termed *dancing synchronization*. Let us use the motion of two

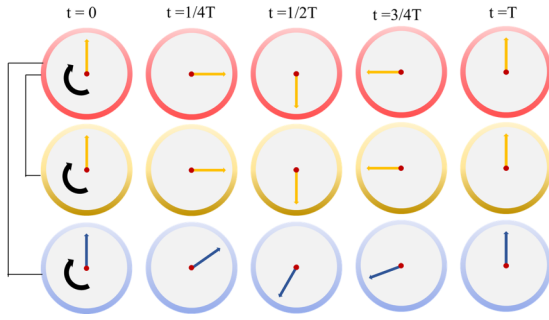*tai.min@xjtu.edu.cn
†phxwan@ust.hk

FIG. 1. Illustration of two types of synchronizations. The red and yellow clocks illustrate a conventional in-phase synchronization. Two clocks point to exactly the same position at all times. The red and blue clocks illustrate a dancing synchronization. Two clocks point to 12 o'clock at $t = 0$ and complete a cycle in exactly 12 h. In between, the two clocks point in different directions most of the time.

coupled clocks, shown in Fig. 1, to explain the differences between conventional synchronizations and dancing synchronizations. The red clock (the first row) is in synchronization with both the yellow clock (the second row) and the blue clock (the third row) with the same periods, say 12 h. The first and second rows (red and yellow clocks) illustrate several moments of two clocks in a conventional synchronization in which two clocks are in phase (always pointing in the same direction at all times). The first and third rows (red and blue clocks) schematically illustrate relative phases of the two clocks in a dancing synchronization where, within one period, the blue clock rotates slower than the red clock in the first and third phases of the period but faster than the red clock in the second and last phases of their period. The distinct difference of the dancing synchronization from the known ones is that the relative phase of the red and blue clocks varies periodically with the synchronized frequency.

This paper is organized as follows. Section II includes the model description of two coupled STNOs, the methodology, and a demonstration of dancing synchronization. Section III shows that dancing synchronization is universal and exists in well-known complex amplitude nonlinear oscillators and Van der Pol oscillators when there are both reactive and dissipative couplings. Then the main results are summarized.

## II. DANCING SYNCHRONIZATION IN COUPLED STNOs

### A. Model and methodology

Our model, as shown in Fig. 2, consists of two nanopillar STNOs coupled through spin waves in the magnetic insulating layer physically connected with STNOs. Each STNO is made from a magnetic multilayer, as shown in Fig. 2(a), which consists of a polarizer of a perpendicularly magnetized layer [e.g., Pt/(Co/Pt)$_5$] to generate spin-polarized current, and a free layer with in-plane magnetization on top of the polarizer separated by either a nonmagnetic metal such as Cu or a nonmagnetic insulator such as MgO. Under the STT due to the spin-polarized current from the polarizer, the spins in the free layer undergo a self-sustained precession. The self-sustained precession can be detected through tunneling
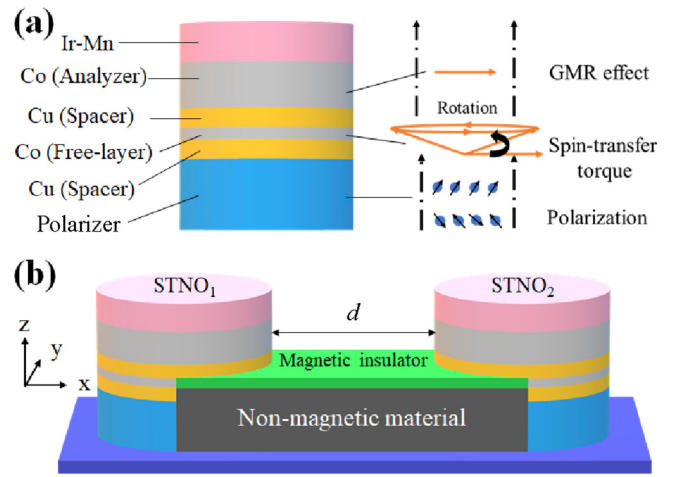


FIG. 2. Sketch of the model. (a) A typical structure of a spin valve in an STNO. Self-sustained precession of spins in the free layer is the result of a limit-cycle solution of the LLG equation under the spin-transfer torque from spin-polarized current that, in turn, is obtained by passing current through the polarizer layer. (b) Two STNOs connected by a magnetic insulating film are coupled by spin waves in the film. $d$ is the distance between two STNOs.

magnetoresistance [40,41] of the analyzer on top of the free layer separated by another nonmagnetic layer such as a thin Cu film. The analyzer is a thick ferromagnetic film whose magnetization is pinned by an antiferromagnetic layer (e.g., Ir-Mn) such that self-sustained magnetization precession of the free layer can generate an oscillatory voltage between the top and bottom layers of the whole nanopillar shown in Fig. 2. Two STNOs have a nominal size of $70 \times 60 \, \text{nm}^2$, and free-layer thickness is 3 nm. The free layer is assumed to be made of Co with a saturation magnetization of $M_{s,\text{Co}} = 886 \, \text{kA/m}$, a magnetic anisotropy coefficient of $K = 4453 \, \text{J/m}^3$ (parallel to the line from the center of the left STNO to the center of the right STNO), an exchange stiffness constant of $A_{\text{Co}} = 25 \, \text{pJ/m}$, and a Gilbert damping constant of $\alpha = 0.02$ [42]. Our two STNOs have slightly different spin polarizations $P$ of $P_1 = 0.38$ for the left STNO and $P_2 = 0.44$ for the right one. The intrinsic oscillation frequencies of the two isolated STNOs under a current density of $1.435 \times 10^7 \, \text{A/cm}^2$ are 9.87 and 10.20 GHz, respectively. An yttrium iron garnet (YIG) film with a thickness of 3 nm connects two STNOs as shown in Fig. 2. The material parameters of YIG are $A_{\text{YIG}} = 4.2 \, \text{pJ/m}$ and $K_{\text{YIG}} = 754 \, \text{J/m}^3$ [43]. The interface (between the YIG film and STNOs) exchange coupling is assumed to be $A_{\text{eff}} = 2A_{\text{Co}}A_{\text{YIG}}/(A_{\text{Co}} + A_{\text{YIG}})$ [44]. Thus, two STNOs couple through spin waves in the YIG film generated by the STNOs [20,27–30], as well as static magnetic interaction [24–26].

Spin precession in STNO free layers will generate and modify spin waves in the YIG film such that two STNOs can interact with each other through the exchange of spin waves. This spin wave mediated coupling is much stronger [29] than the direct magnetic-dipole interactions between two STNOs when they are close to each other. The STNO separation, material parameters, and applied electrical current can be used to control the effective coupling of STNOs. We investigate
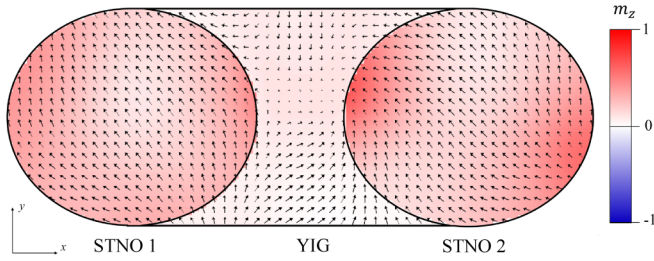
FIG. 3. A snapshot of the spin distribution of the system in synchronization. The arrows denote the direction of the in-plane component of magnetization, and the color encodes the information about $m_z$.

the spin dynamics of the hybrid structure consisting of free layers of STNOs and the YIG film under the injection of spin-polarized currents. The current density has a nonzero value only within the free layers of STNOs. The thermal effect, the field generated from the analyzer layer (not show), and the field induced by charge current are ignored. The spin dynamics of the system is governed by the Landau-Lifshitz-Gilbert (LLG) equation,

$$\frac{d\mathbf{m}}{dt} = -\gamma \mathbf{m} \times \mathbf{H}_{\text{eff}} + \alpha \left( \mathbf{m} \times \frac{d\mathbf{m}}{dt} \right) + a(\mathbf{m} \times \mathbf{m}_{\text{p}} \times \mathbf{m}), \tag{1}$$

where $\mathbf{m}$, $\gamma$, $t$, and $\mathbf{H}_{\text{eff}}$ are, respectively, the unit vector of the magnetization, gyromagnetic ratio, the time, and the effective magnetic field, $\mathbf{H}_{\text{eff}} = \frac{2A}{\mu_0 M_s} \nabla^2 \mathbf{m} + \frac{2K}{\mu_0 M_s} m_z \hat{z} + \mathbf{H}_d$, which includes the exchange field, the anisotropic field, and the demagnetizing field $\mathbf{H}_d$. Coefficient $a = |\frac{\hbar}{\mu_0 e}| \frac{J}{dM_s} \frac{P\lambda^2}{(\lambda^2+1)+(\lambda^2-1)(\mathbf{m}\cdot\mathbf{m}_p)}$ describes the Slonczewski torque, where $\hbar$, $d$, $M_s$, $J$, $e$, $\mu_0$, and $P$ are the reduced Planck constant, the thickness of the free layer, the saturation magnetization of the free layer, the charge current density, the electron charge, the vacuum permeability, and the polarization of the charge current, respectively. Under a proper spin-polarized current, the spins in the free layer undergo a self-sustained precession. Equation (1) for the whole hybrid system of the YIG film and free layers in STNOs is numerically solved by using the Object Oriented MicroMagnetic Framework (OOMMF) [44]. To balance the speed and accuracy, the cell size used in this study is $1 \times 1 \times 3$ nm$^3$.

Initially, spins of the left STNO are all along the $x$ direction, and all spins of the right STNO are in the $yz$ plane and 45° away from the $z$ axis. Under an electric current density of $1.435 \times 10^7$ A/cm$^2$, two STNOs are synchronized after a few nanoseconds when the distance between STNOs is $d = 22$ nm. Figure 3 is a typical snapshot of the spin configuration of two STNOs in the synchronization where spins in both STNOs and YIG do not align along the same direction even in the synchronized state because of the edge and interface effect.

### B. Coupling length of the STNOs with the spin wave in YIG

We first study the coupling distance of the two STNOs through the spin waves in the YIG film. We use OOMMF to simulate two systems identical to the one described above ex-
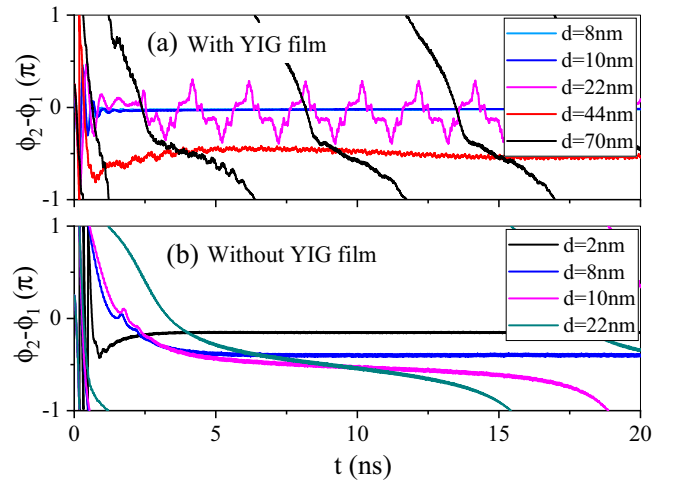


FIG. 4. Time evolution of phase differences (a) with spin-wave coupling and (b) with only dipolar coupling for various distances and a fixed charge current density of $1.435 \times 10^7$ A/cm$^2$.

cept that one of them does not have the YIG film such that two STNOs couple to each other through the dipolar field. Thus, one can attribute the difference in the two systems to the spin wave mediated coupling. To see different behaviors of the two systems, we collect time evolution data of the average magnetization $\mathbf{m}_i(t)$ of two STNOs, where $i = 1, 2$ label the two STNOs. The angles of the in-plane component of $\mathbf{m}_i(t)$ with the $x$ axis are denoted $\phi_i(t)$. The time dependence of the phase difference $\phi_2(t) - \phi_1(t)$ can tell synchronizations from non-synchronizations. $\phi_2(t) - \phi_1(t)$ varies over the $2\pi$ range in a nonsynchronized motion, while it is constant in a conventional synchronization. Our OOMMF simulation results are shown in Fig. 4(a) for system with a YIG film and in Fig. 4(b) for system without a YIG film. Indeed, both nonsynchronizations [for $d = 70$ nm in Fig. 4(a) and $d = 10, 22$ nm in Fig. 4(b)] and conventional synchronizations [for $d = 8, 10, 44$ nm in Fig. 4(a) and $d = 2, 8$ nm in Fig. 4(b)] can be clearly identified. Interestingly, a periodically oscillating $\phi_2(t) - \phi_1(t)$ with an amplitude of 60° appears at $d = 22$ nm in the case in which two STNOs are coupled by both dipolar field and the spin waves due to the YIG film. This is exactly the dancing synchronization discussed earlier. Without the spin waves, such a synchronization was not observed [Fig. 4(b)]. Therefore, results in Fig. 4 demonstrate not only that the coupling distance between two STNOs by spin waves becomes much longer (44 nm) than that (8 nm) by the dipolar field but also that it can induce a different type of synchronization. Below, we will examine this type of synchronization more closely.

### C. Dancing synchronization

For the dancing synchronization at $d = 22$ nm and under current density of $1.435 \times 10^7$ A/cm$^2$, we plot the time evolutions of $m_{1x}(t)$ (blue curve) and $m_{2x}(t)$ (red curve), $x$ components of the average magnetization of the free layer in the left and right STNOs, respectively, in Fig. 5(a). The two curves are periodic with the same period but have different shapes, i.e., $m_{\alpha x}(t) = m_{\alpha x}(t + nT)$ ($\alpha = 1, 2$), where $T$ is the period and $n$ is an arbitrary integer. For example,
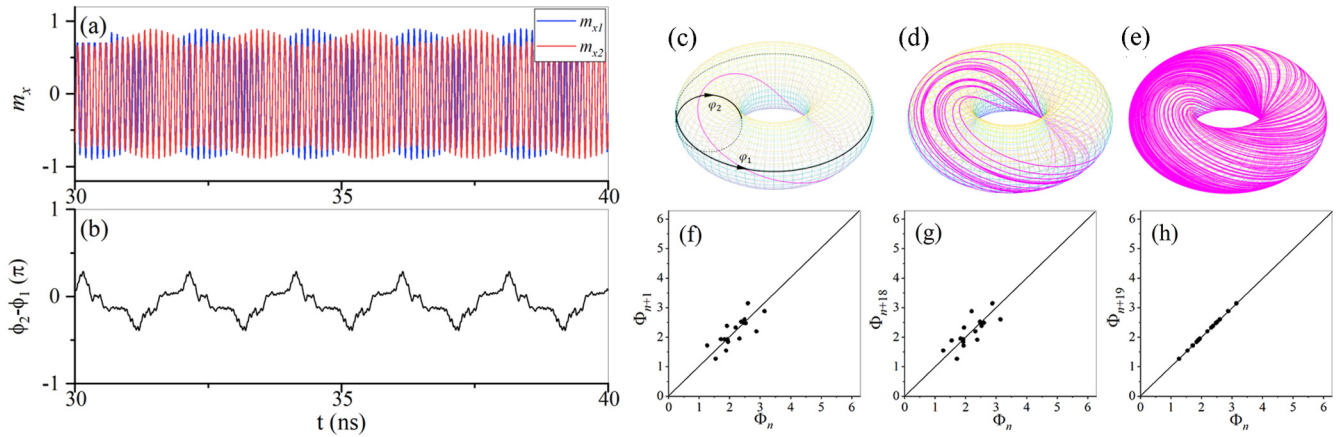
FIG. 5. (a) Time evolutions of $m_{1x}(t)$ (blue curve) and $m_{2x}(t)$ (red curve) in a dancing synchronization: $m_{1x}(t)$ and $m_{2x}(t)$ show fast and slow motions, respectively (in nanoseconds). The relative phase of the red and blue curves varies with a much longer common period. (b) Time evolution of the phase difference in the dancing synchronization. The common long period is about 2 ns, much longer than a 0.1 ns oscillation. (c)–(e) Phase trajectories $\phi_2(\phi_1)$ of two STNOs on the $\phi_1\phi_2$ torus ($\phi_1$ for the large circle and $\phi_2$ for the smaller one) under a current density of $1.435 \times 10^7$ A/cm$^2$; (c) is for a conventional in-phase synchronization when the distance is 10 nm, (d) is for the dancing synchronization in which $\phi_2(\phi_1)$ returns to its starting point after 19 turns when the distance is 22 nm, and (e) is for a nonsynchronized state in which $\phi_2(\phi_1)$ never closes when the distance is 70 nm. (f)–(h) $\Phi_n = \phi_2(\phi_1 = \pi)$ is the value of $\phi_2$ in the Poincaré maps. (f)–(h) are, respectively, for $\Phi_n$ vs $\Phi_{n+1}$, $\Phi_n$ vs $\Phi_{n+18}$, and $\Phi_n$ vs $\Phi_{n+19}$.

within one common period, both $m_{1x}(t)$ and $m_{2x}(t)$ oscillate 19 times with different amplitudes before returning to their initial values. This phenomenon is different from the conventional in-phase synchronization, where time evolutions of $m_{1x}(t)$ and $m_{2x}(t)$ either overlap completely with each other or differ by a fixed lag. Figure 5(b) plots the time evolution of the phase difference $\phi_2(t) - \phi_1(t)$ of the two STNOs. Clearly, $\phi_2(t) - \phi_1(t)$ oscillates periodically with an amplitude of about $\pi/3$ and a period of 2 ns. This is different from all known synchronizations where $\phi_2(t) - \phi_1(t)$ is a constant. Because of this periodical variation of the relative phase of the two STNOs that is reminiscent of two partners dancing in rhythm with different arm movements, we term this observed synchronization dancing synchronization.

To further prove the dancing synchronization in Fig. 5(a), we plot trajectory $\phi_2(\phi_1)$ on the $\phi_1\phi_2$ torus, as shown in Figs. 5(c)–5(e). In a conventional synchronization where $\phi_2(t) - \phi_1(t) = $ const, $\phi_2(t)$ and $\phi_1(t)$ change by $2\pi$ simultaneously, so that $\phi_2(\phi_1)$ is a simple one-turn closed curve as shown in Fig. 5(c). This is the case when the distance between the two STNOs is 10 nm under a current density of $1.435 \times 10^7$ A/cm$^2$. The case of $d = 22$ nm at the same current density is fundamentally different, as shown in Fig. 5(b). $\phi_2(t) - \phi_1(t)$ is not constant and varies periodically with a longer period. The trajectory is still a closed curve, as shown in Fig. 5(d), which displays data in Fig. 5(a) as $\phi_2(\phi_1)$ on the $\phi_1\phi_2$ torus. $\phi_2(\phi_1)$ returns to its starting point after 19 turns. If $\phi_1(t)$ and $\phi_2(t)$ either are not periodic or do not have a common period, the trajectory will not be a closed curve and will fill up the $\phi_1\phi_2$ torus, as shown in Fig. 5(e), which illustrates the motion of the two STNOs for $d = 70$ nm and under a current density of $1.435 \times 10^7$ A/cm$^2$.

One can further confirm the dancing synchronization of two STNOs in Fig. 5(a) via the Poincaré maps. In the map, $\Phi_n$ is defined as angle $\phi_2$ modulo $2\pi$ when $\phi_1 = (2n - 1)\pi$, i.e., $\{\Phi_n = \phi_2(\phi_1 = (2n - 1)\pi) \bmod 2\pi | n = 1, 2, \ldots\}$. $\Phi_n$ can be

grouped into various sets such as $\{(\Phi_n, \Phi_{n+1}) | n = 1, 2, \ldots\}$, $\{(\Phi_n, \Phi_{n+18}) | n = 1, 2, \ldots\}$, and $\{(\Phi_n, \Phi_{n+19}) | n = 1, 2, \ldots\}$. These three sets are plotted in Figs. 5(f)–5(h), where the $x$ axis is for $\Phi_n$ and the $y$ axis is for $\Phi_{n+N}$, $n = 1, 2, 3, \ldots$. $\{(\Phi_n, \Phi_{n+N}) | n = 1, 2, \ldots\}$ fall onto the line of $\Phi_{n+N} = \Phi_n$ if $\phi_1$ and $\phi_2$ have a common period of $N$ turns. This is exactly the case here with $N = 19$, as shown in Fig. 5(h). As a comparison, sets with $N = 1$ and 18 are off the straight line, as shown in Figs. 5(f) and 5(g).

### D. Robustness of the dancing synchronization

The observed dancing synchronization is very robust and can exist in a finite region in the parameter space. For example, Figs. 6(a1)–6(a5) show the time evolution of $\phi_2(t) - \phi_1(t)$ for various $d$ at a fixed current density of $J = 1.435 \times 10^7$ A/cm$^2$ while all other parameters remain the same as those in Fig. 5. Clearly, the dancing synchronization, featured by the periodic variation of $\phi_2(t) - \phi_1(t)$, occurs in the window of $d = 18$–23 nm. Similarly, we observe the dancing synchronization at fixed $d = 22$ nm in the current density window of $J = 1.41$–1.48 $\times 10^7$ A/cm$^2$ while all other parameters remain the same as those in Fig. 5 in Figs. 6(b1)–6(b5), whereas $\phi_2(t) - \phi_1(t)$ in Figs. 6(b2)–6(b4) vary periodically. Moreover, as shown in Fig. 6(c2) at a fixed $d = 22$ nm, $J = 1.435 \times 10^7$ A/cm$^2$, the dancing synchronization occurs when the magnetic anisotropy direction and its magnitude vary. Interestingly, the dancing synchronization exists even in the absence of the anisotropy, as shown in Fig. 6(c1).

A natural question is whether the dancing synchronization can still survive when the so-called fieldlike torque is included in Eq. (1). The answer is yes, as shown in Fig. 7(a) for $d = 22$ nm and under a current density of $1.45 \times 10^7$ A/cm$^2$ with 45% fieldlike torque. The torque modifies slightly the details of the synchronization. The dancing synchronization
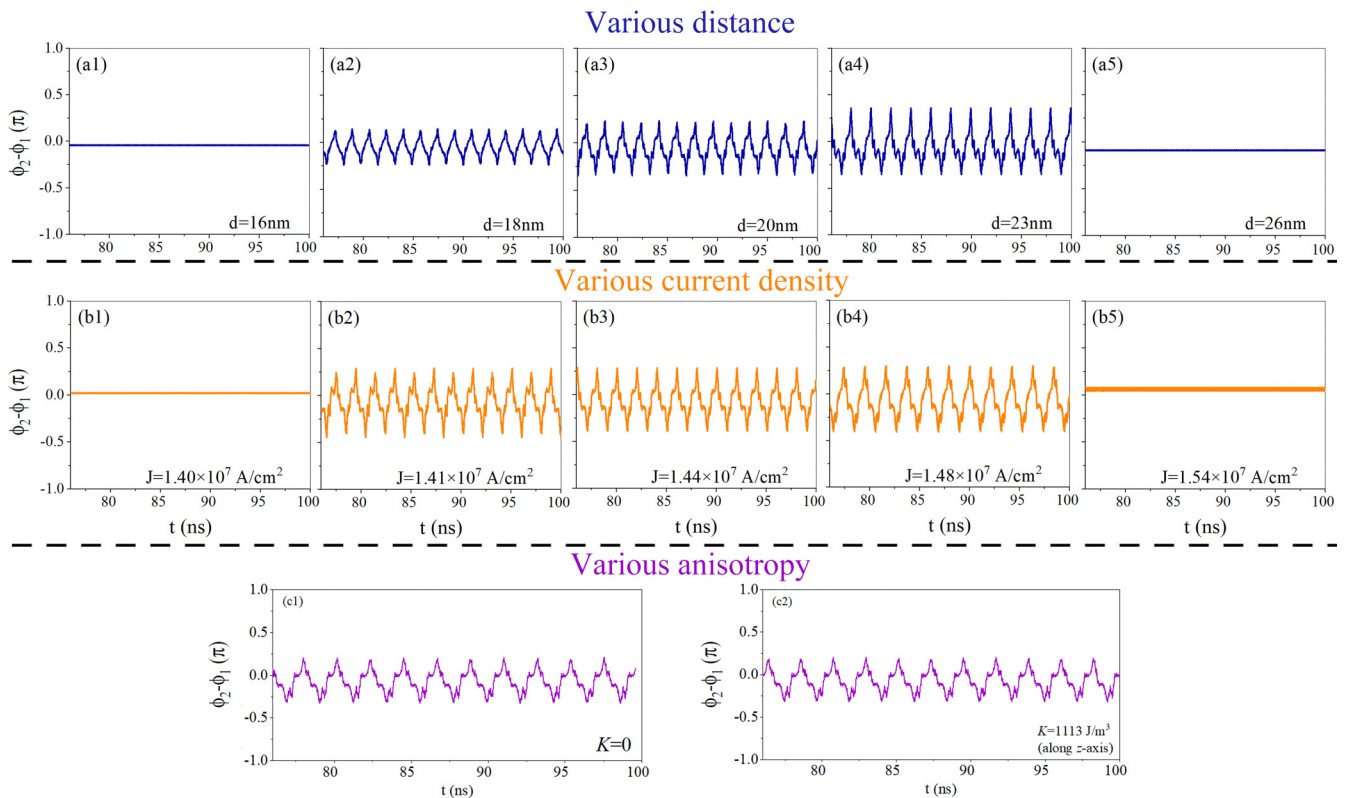
FIG. 6. Time evolution of phase differences for various distances $d$ at a fixed charge current $J = 1.435 \times 10^7$ A/cm², for various charge currents $J$ at a fixed distance $d = 22$ nm, and for different conductions of the magnetic anisotropy at fixed $d = 22$ nm and $J = 1.435 \times 10^7$ A/cm². All other parameters are the same as those used in Fig. 5.

is still observed even when an additional external magnetic field up to 0.3 mT along the $z$ axis is applied, as shown in Fig. 7(b) for 0.1 mT. These results demonstrate the robustness of the dancing synchronization against different parameters and different types of torques.

The observed dancing synchronization is not a transient process, which can be verified by a much longer micromagnetic simulation of 300 ns. In this simulation, we set

$d = 22$ nm and $K_{YIG} = 0$ in order to show that the dancing synchronization is robust against variation of spin waves that glue two STNOs together. The rest of the model parameters are the same as those in Fig. 5. As shown in Fig. 8, there is no sign that the dancing synchronization changes to another type of motion. Evolution of the phase difference between $t = 290$ ns and $t = 300$ ns is the same as that between $t = 30$ ns and $t = 40$ ns and is very similar to Fig. 5(b) with $K_{YIG} \neq 0$.
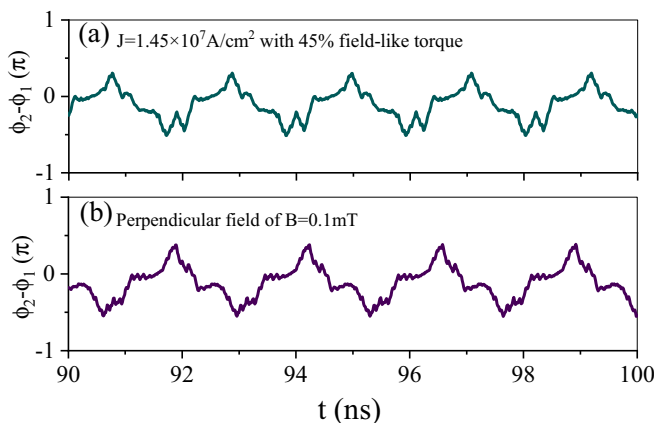


FIG. 7. Time evolution of phase differences at a fixed distance $d = 22$ nm and (a) under a current density of $1.45 \times 10^7$ A/cm² with 45% fieldlike torque or (b) under an external perpendicular magnetic field of 0.1 mT. All other parameters are the same as those in Fig. 5.
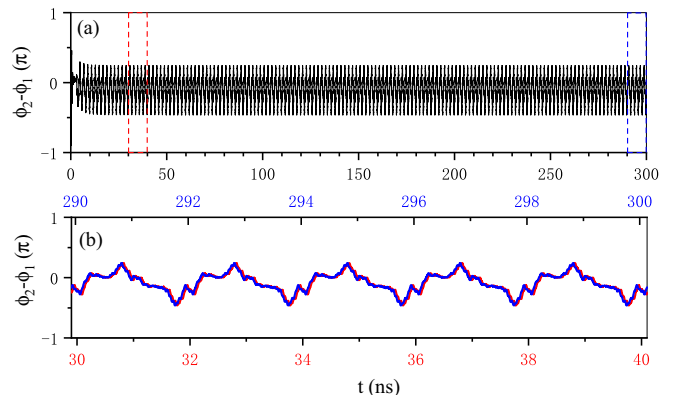


FIG. 8. (a) A 300 ns long evolution of phase differences at $d = 22$ nm and $K_{YIG} = 0$ under current density of $1.435 \times 10^7$ A/cm². (b) Zoom of the evolutions in $t = 30$–$40$ ns (bottom axis and red curve) and in $t = 290$–$300$ ns (top axis and blue curve). Two curves overlap with each other, showing no sign of a transient motion.
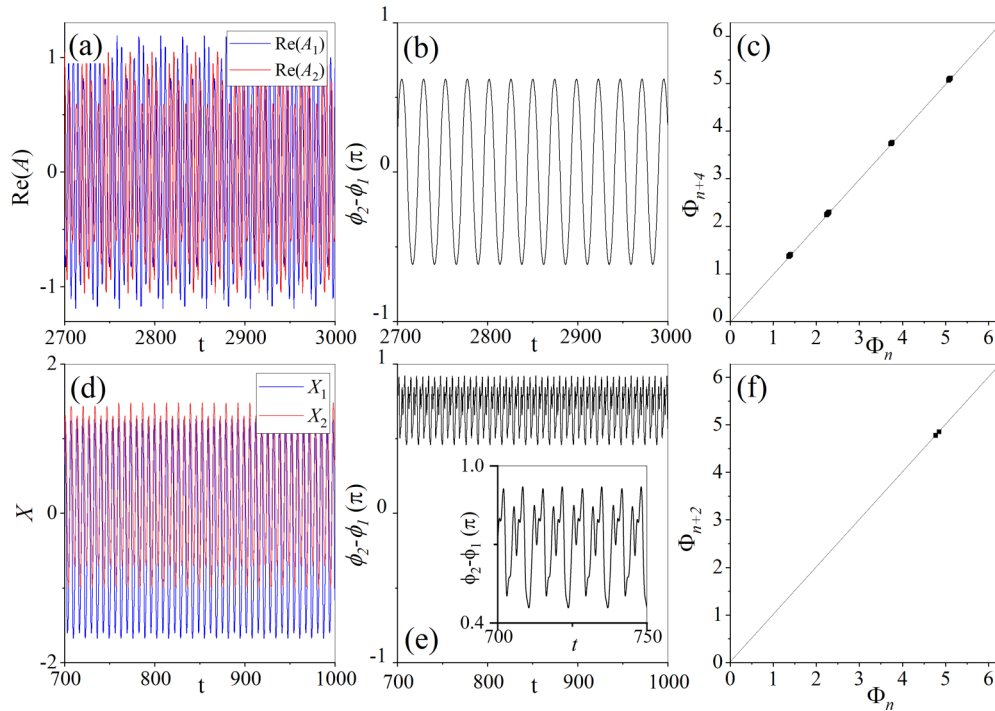
FIG. 9. Dancing synchronizations in a complex amplitude model and a Van der Pol model. (a)–(c) are the time evolution of complex amplitudes, phase difference, and the Poincaré map in the complex amplitude model, respectively. (d)–(f) are the real-time trace of two oscillators' amplitudes, the time evolution of the phase difference, and the Poincaré map in the VdP model, respectively.

## III. DANCING SYNCHRONIZATION IN TOY MODELS

Importantly, genuine physics phenomena should be universal. In order to demonstrate that the dancing synchronization can also appear in well-known and well-studied popular models, we consider two coupled complex variable oscillators [11] and two coupled Van der Pol oscillators. The two models have been intensively studied by numerous people before. A close examination of earlier studies shows that most people use the simple linear reactive coupling (a function of only the oscillator position) between two nonlinear oscillators. Indeed, we did not observe the dancing synchronization with only linear reactive or linear dissipative coupling (involving oscillator velocities) like in previous studies. However, when two nonlinear oscillators couple with each other both reactively and dissipatively, dancing synchronization appears. Below, we report our findings.

### A. Dancing synchronization in coupled complex variable oscillators

We first search dancing synchronization in the complex variable oscillation model used by Matheny and coworkers [11], who reported various fragmentation synchronizations. The nonlinear dynamical equations for $n$ complex variables $A_j(t)$ $(j = 1, \ldots, n)$ read

$$\dot{A}_j = \lambda A_j(1 - |A_j|) + i(\omega_j A_j + \alpha |A_j|^2 A_j)$$
$$+ i\beta \sum_{k \neq j}^{n} (A_k - A_j) + \gamma \sum_{k \neq j}^{n} A_k(1 - |A_j|), \quad (2)$$

where $\alpha$ is the nodal nonlinearity that couples frequency to amplitude, $\beta$ measures the strength of reactive coupling among a pair of oscillators, and $\gamma$ is a nonlinear coupling. Each complex variable $A_j(t)$ stands for an oscillator. The real part of $A_j(t)$ represents a real variable which can be observed in the oscillation. Equation (2) is often used to introduce the concept of synchronization [1]. For STNOs, $A_j(t)$ can be $\mathbf{m}_j$. The phase of each oscillator $\phi_j(t)$ is defined as the argument of $A_j$. For $\gamma = 0$, the model has been used to describe various nonlinear systems, including nanoelectromechanical systems (NEMS) [11]. This model is sometimes called "a universal model for self-sustained oscillations" in comparison to the Kuramoto model [9] widely used to describe "phase synchronization" of coupled oscillators or networks. In the Kuramoto model, an oscillator is represented by only one real variable.

Various nonlinear phenomena such as self-sustained oscillation and fragmentation synchronizations have been obtained from Eq. (2) with $\gamma = 0$ [11], but not the dancing synchronization. We show now that the dancing synchronization of two complex variable oscillators can exist for certain $\gamma \neq 0$. The numerical solutions of Eq. (2) from the fourth-order Runge-Kutta method are plotted in Figs. 9(a) and 9(b) for $\gamma = 0.01$, $\omega_1 = 0.5$ Hz, $\omega_2 = 0.7$ Hz, $\alpha = 0.59126$, $\beta = 0.056$, and $\lambda = 0.01$, with the initial conditions $A_1(0) = 2.51e^{0.16i}$ and $A_2(0) = 1.62e^{0.79i}$. Like in the STNO system, the amplitudes $Re(A_1)$ and $Re(A_2)$, as shown in Fig. 9(a), oscillate with a long common period of 24.75 s. The phase difference $\phi_2(t) - \phi_1(t)$, as shown in Fig. 9(b), is not constant and varies with the same synchronized period of 24.75 s with an amplitude of $0.6\pi$. Because all nonlinear dynamical systems have gain and loss, the properties of attractors do not depend on the

initial states. The dancing synchronization is also checked using the phase trajectory and the Poincaré map $\{\Phi_n = \phi_2(\phi_1 = (2n - 1)\pi)$ mod $2\pi | n = 1, 2, \ldots\}$, and the phase trajectory $\phi_2(\phi_1)$ is closed after four turns on the $\phi_1\phi_2$ torus, as demonstrated by the points $\{(\Phi_n, \Phi_{n+4}) | n = 1, 2, \ldots\}$ on the line $y = x$ in Fig. 9(c).

### B. Dancing synchronization in two coupled Van der Pol oscillators

We have also demonstrated the existence of the dancing synchronization in two coupled Van der Pol (VdP) nonlinear oscillators. The VdP equation is not only a popular model for demonstrating the self-sustained oscillation in nonlinear systems [45,46] but also realizable by *RCL* circuits with a negative differential resistor. The standard VdP equation is

$$\ddot{x}_i + \mu(x_i^2 - A_i)\dot{x}_i + \omega_i^2 x_i = -f_{i, j \neq i}, \quad (3)$$

where $i, j = 1, 2$ label two oscillators and $\mu > 0$ is a parameter measuring energy gain ($x_i^2 < A_i$) and energy loss ($x_i^2 > A_i$). $A_i > 0$ specifies the size of the energy gain region and is roughly the oscillation amplitude. $\omega_i$ and $f_{ij}$ describe, respectively, the oscillatory frequency and the coupling between oscillators $i$ and $j$. Coupled VdP oscillators have been intensively studied before with either reactive or dissipative coupling [47,48]. Interestingly, only conventional synchronizations were reported in all earlier studies of coupled VdP oscillators. Here we show that the dancing synchronization can appear in coupled VdP oscillators with both reactive and dissipative couplings,

$$f_{ij} = \alpha(x_j - x_i) + (j - i)\beta\sqrt{|x_i x_j + \dot{x}_i \dot{x}_j - 1|}, \quad (4)$$

where the first term is a reactive coupling and the second one is dissipative. Figure 9(d) shows the numerical solutions of Eq. (3) from the fourth-order Runge-Kutta method for $\mu = 1$, $A_1 = A_2 = 0.5$, $\omega_1 = 1\,\text{Hz}$, $\omega_2 = 0.98\,\text{Hz}$, $\alpha = 0.12$, $\beta = 0.30$. The final self-sustained oscillations shown in Fig. 9(d) do not depend on the initial conditions. Two oscillators have distinguished appearances but share a common long period of $13.19\,\text{s}$. To see clearly that this is a dancing synchronization, we define

$$\phi_j(t) = \int_0^t \frac{\dot{x}_j(\tau)\dddot{x}_j(\tau) - \ddot{x}_j(\tau)^2}{\dot{x}_j(\tau)^2 - \ddot{x}_j(\tau)^2} \, d\tau, \quad (5)$$

which is the total winding angle of $(x(t), \dot{x})$ in the $x\dot{x}$ phase plane. $\phi_2 - \phi_1$ varies periodically with an amplitude of around $0.2\pi$ within the common long period of $13.19\,\text{s}$, as plotted in Fig. 9(e). Again, the dancing synchronization is checked using the phase trajectory and the Poincaré map $\{\Phi_n = \phi_2(\phi_1 = (2n - 1)\pi)$ mod $2\pi | n = 1, 2, \ldots\}$, and the phase trajectory $\phi_2(\phi_1)$ is closed after two turns on the $\phi_1\phi_2$ torus, as demonstrated by the points $\{(\Phi_n, \Phi_{n+2}) | n = 1, 2, \ldots\}$ on line $y = x$ in Fig. 9(f).

### C. Discussion

Simple toy models allow one to test key ingredients for a new phenomenon, which is the case here. In order to demonstrate the importance of nonlinear coupling between two oscillators, we set $\gamma = 0$ for model (2) and $\beta = 0$
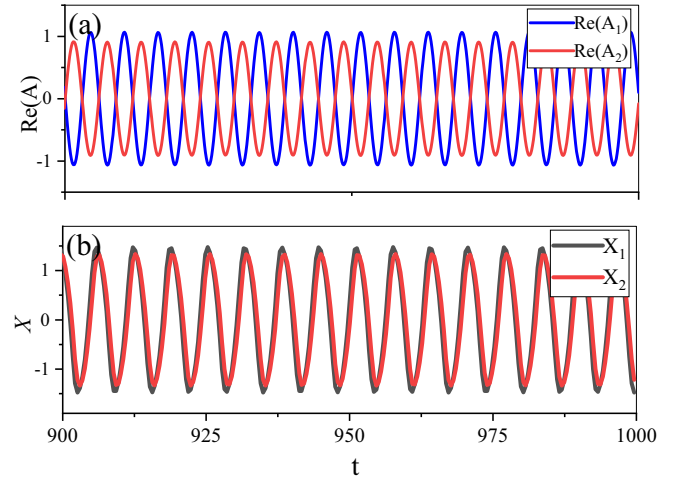


FIG. 10. Time evolution of two nonlinear oscillators for (a) the complex amplitude model with $\gamma = 0$ and (b) the Van der Pol model with $\beta = 0$.

for model (3). In both cases, we were not able to find any trace of dancing synchronization within many trials. Figure 10 shows what was typically observed with only conventional synchronizations, where Fig. 10(a) is the result of model (2) with $\gamma = 0$ and Fig. 10(b) is for model (3) with $\beta = 0$ while all other parameters are the same as those in Fig. 9 that show dancing synchronizations. Our studies show the importance of nonlinear couplings for the dancing synchronization.

The dancing synchronization in the toy models is also robust against a certain degree of variation of parameters. As an example, in model (2) when the intrinsic frequency of the second oscillator and $\alpha$ change from 0.7 to 0.8 and from 0.59126 to 0.55207, respectively, dancing synchronization also appears, as shown in Figs. 11(a1)–11(a3), in which the state returns to its starting point after moving around the origin of the phase plane for five turns [Fig. 11(a3)]. Similarly, if we change the intrinsic frequency of the second oscillator from 0.7 to 0.9 and $\alpha$ from 0.59126 to 0.59445, dancing synchronization is still there, as shown in Figs. 11(b1)–11(b3), in which the state returns to its starting point after six turns [Fig. 11(b3)].

A true natural phenomenon should tolerate thermal noise. To demonstrate that our dancing synchronization is insensitive to the thermal noise, we add a stochastic force to the original equations; for example, the nonlinear dynamical equation of the complex amplitude model becomes

$$\dot{A}_j = \lambda A_j(1 - |A_j|) + i(\omega_j A_j + \alpha|A_j|^2 A_j)$$
$$+ i\beta \sum_{k \neq j}^n (\widetilde{A}_k - A_j) + \gamma \sum_{k \neq j}^n \widetilde{A}_k(1 - |A_j|), \quad (6)$$

and the Van der Pol model becomes

$$f_{ij} = \alpha(\widetilde{x}_j - x_i) + (j - i)\beta\sqrt{|x_i\widetilde{x}_j + \dot{x}_i\dot{x}_j - 1|}, \quad (7)$$

where $\widetilde{A}_k = A_k + aS(t)$ and $\widetilde{x}_j = x_j + aS(t)$, where $S(t)$ is a standard Gaussian stochastic process and $a$ measures the strength of random force. In simulations, an independent
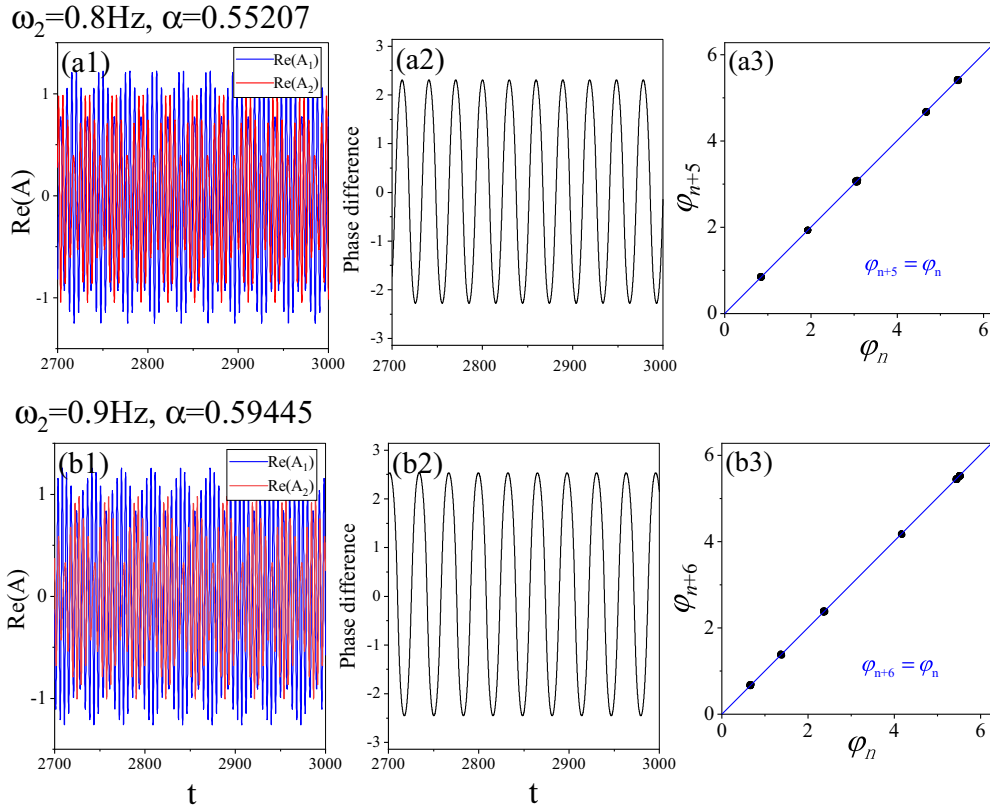
FIG. 11. Dancing synchronization of model (2) with (a) $\omega_2 = 0.8$ Hz, $\alpha = 0.55207$ and (b) $\omega_2 = 0.9$ Hz, $\alpha = 0.59445$. Panels from left to right are the time evolution of the two oscillators, the corresponding phase difference, and the Poincaré map.

Gaussian-distributed random force of standard deviation $\sigma = 1$ is assigned in each step ($\Delta t = 4.7 \times 10^{-3}$ s). We solved equations numerically with $a = 1 \times 10^{-7}$ and $a = 5 \times 10^{-7}$. The results of the complex amplitude model and the Van der Pol model are displayed in Fig. 12. The Poincaré map (collecting data from 3000 periods) is slightly dispersed for both $a$. All return points fall around the line $\varphi_{n+4} = \varphi_n$, which sustains our statement on the robustness of the dancing
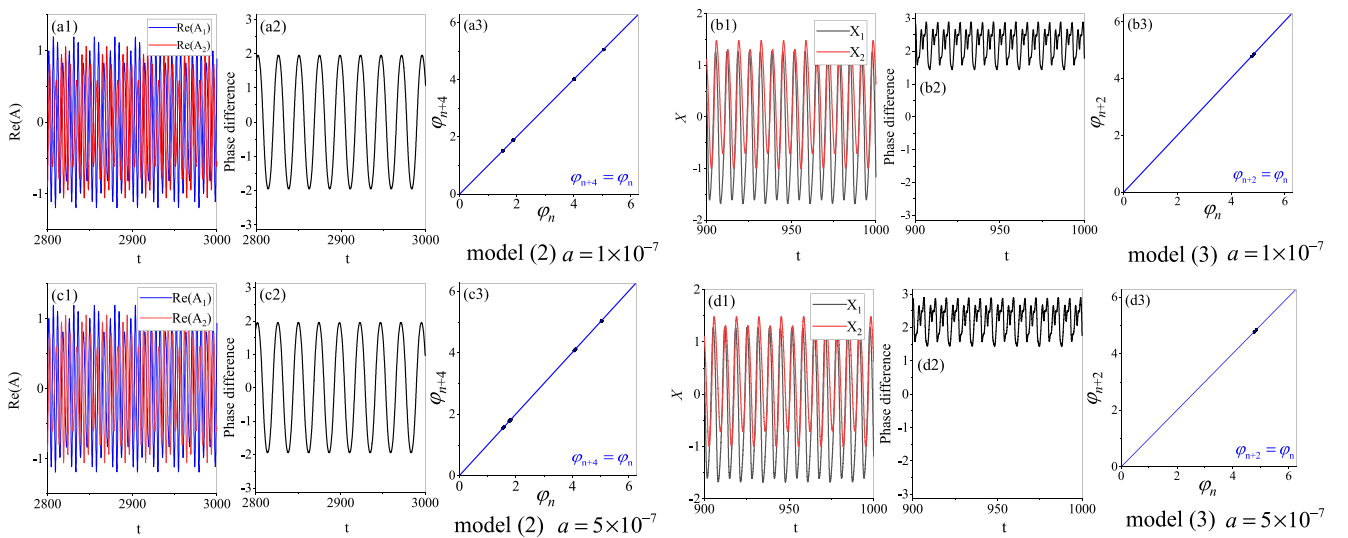


FIG. 12. Dancing synchronization of the complex amplitude model [model (2)] (a1)–(a3) for $a = 1 \times 10^{-7}$ and (c1)–(c3) for $a = 5 \times 10^{-7}$ and the Van der Pol model [model (3)] (b1)–(b3) for $a = 1 \times 10^{-7}$ and (d1)–(d3) for $a = 5 \times 10^{-7}$. (a1), (b1), (c1), and (d1) are the time evolution of two oscillators. (a2), (b2), (c2), and (d2) are the time evolution of the phase difference. (a3), (b3), (c3), and (d3) are the Poincaré map. The periodical oscillation of the phase difference and the Poincaré map demonstrate the dancing synchronization under the noise.

synchronizations. The dancing synchronization of the Van de Pol model is much more resilient than that of the complex amplitude model, as shown in Figs. 12(b) and 12(d), with $a = 1 \times 10^{-7}$ and $a = 5 \times 10^{-7}$, respectively.

## IV. CONCLUSION

In summary, a type of synchronization, termed dancing synchronization, was observed in two STNOs coupled through spin waves and the static magnetic interaction. The two STNOs oscillate with the same period, and their relative phase difference varies periodically with a common long period, different from all known synchronizations in which the relative phases of two nonlinear oscillators are fixed. We further demonstrated that the dancing synchronization is a general phenomenon that can also occur in the complex variable oscillation model used by Matheny and coworkers

[11] and in two coupled Van der Pol oscillators, as long as they are coupled reactively and dissipatively. The dancing synchronization exists in a narrow parameter region between nonsynchronization and in-phase synchronization of two nonlinear oscillators.

[1] S. H. Strogatz, *Nonlinear Dynamics and Chaos* (Addison-Wesley Publishing Company, Reading, Massachusetts, 1994).

[2] A. Pikovsky, M. Rosenblum, and J. Kurths, *Synchronization: A Universal Concept in Nonlinear Sciences* (Cambridge University Press, Cambridge, 2001).

[3] I. Z. Kiss, Y. Zhai, and J. L. Hudson, Science **296**, 1676 (2002).

[4] G. Buzsáki and A. Draguhn, Science **304**, 1926 (2004).

[5] B. H. Repp and Y.-H. Su, Psychon. Bull. Rev. **20**, 403 (2013).

[6] P. W. Anderson, Science **177**, 393 (1972).

[7] H. C., Letters to Sluse, no. 1333 of 24 February 1665, no. 1335 of 26 February 1665, no. 1345 of 6 March 1665 (Société Hollandaise des Sciences, Martinus Nijhoff, La Haye, 1893).

[8] F. Varela, J.-P. Lachaux, E. Rodriguez, and J. Martinerie, Nat. Rev. Neurosci. **2**, 229 (2001).

[9] J. A. Acebrón, L. L. Bonilla, C. J. Pérez Vicente, F. Ritort, and R. Spigler, Rev. Mod. Phys. **77**, 137 (2005).

[10] L. Huang, K. Park, Y.-C. Lai, L. Yang, and K. Yang, Phys. Rev. Lett. **97**, 164101 (2006).

[11] M. H. Matheny, J. Emenheiser, W. Fon, A. Chapman, A. Salova, M. Rohden, J. Li, M. Hudoba de Badyn, M. Pósfai, L. Duenas-Osorio, M. Mesbahi, J. P. Crutchfield, M. C. Cross, R. M. D'Souza, and M. L. Roukes, Science **363**, eaav7932 (2019).

[12] M. Zahedinejad, H. Mazraati, H. Fulara, J. Yue, S. Jiang, A. A. Awad, and J. Åkerman, Appl. Phys. Lett. **112**, 132404 (2018).

[13] A. A. Awad, P. Dürrenfeld, A. Houshang, M. Dvornik, E. Iacocca, R. K. Dumas, and J. Åkerman, Nat. Phys. **13**, 292 (2017).

[14] J. Slonczewski, J. Magn. Magn. Mater. **159**, L1 (1996).

[15] L. Berger, Phys. Rev. B **54**, 9353 (1996).

[16] X. R. Wang and Q. Niu, Phys. Rev. B **59**, R12755 (1999).

[17] X. R. Wang, J. N. Wang, B. Q. Sun, and D. S. Jiang, Phys. Rev. B **61**, 7261 (2000).

[18] Z. Z. Sun and X. R. Wang, Phys. Rev. B **74**, 132401 (2006).

[19] Z. Z. Sun and X. R. Wang, Phys. Rev. B **73**, 092416 (2006).

[20] A. Slavin, Nat. Nanotechnol. **4**, 479 (2009).

[21] S. I. Kiselev, J. C. Sankey, I. N. Krivorotov, N. C. Emley, R. J. Schoelkopf, R. A. Buhrman, and D. C. Ralph, Nature (London) **425**, 380 (2003).

[22] S. Kaka, M. R. Pufall, W. H. Rippard, T. J. Silva, S. E. Russek, and J. A. Katine, Nature (London) **437**, 389 (2005).

[23] J. Grollier, V. Cros, and A. Fert, Phys. Rev. B **73**, 060409(R) (2006).

[24] H.-H. Chen, C.-M. Lee, Z. Zhang, Y. Liu, J.-C. Wu, L. Horng, and C.-R. Chang, Phys. Rev. B **93**, 224410 (2016).

[25] A. D. Belanovsky, N. Locatelli, P. N. Skirdkov, F. Abreu Araujo, J. Grollier, K. A. Zvezdin, V. Cros, and A. K. Zvezdin, Phys. Rev. B **85**, 100409(R) (2012).

[26] H. B. Huang, X. Q. Ma, Z. H. Liu, C. P. Zhao, and L. Q. Chen, AIP Adv. **3**, 032132 (2013).

[27] R. K. Dumas and J. Åkerman, Nat. Nanotechnol. **9**, 503 (2014).

[28] S. Sani, J. Persson, S. M. Mohseni, Y. Pogoryelov, P. K. Muduli, A. Eklund, G. Malm, M. Käll, A. Dmitriev, and J. Åkerman, Nat. Commun. **4**, 2731 (2013).

[29] A. Ruotolo, V. Cros, B. Georges, A. Dussaux, J. Grollier, C. Deranlot, R. Guillemet, K. Bouzehouane, S. Fusil, and A. Fert, Nat. Nanotechnol. **4**, 528 (2009).

[30] A. N. Slavin and V. S. Tiberkevich, Phys. Rev. B **74**, 104401 (2006).

[31] M. R. Pufall, W. H. Rippard, S. E. Russek, S. Kaka, and J. A. Katine, Phys. Rev. Lett. **97**, 087206 (2006).

[32] V. Puliafito, G. Consolo, L. Lopez-Diaz, and B. Azzerboni, Physica B (Amsterdam, Neth.) **435**, 44 (2014).

[33] V. Tiberkevich, A. Slavin, E. Bankowski, and G. Gerhart, Appl. Phys. Lett. **95**, 262505 (2009).

[34] A. R. Safin, N. N. Udalov, and M. V. Kapranov, Eur. Phys. J.: Appl. Phys. **67**, 20601 (2014).

[35] R. Lebrun, S. Tsunegi, P. Bortolotti, H. Kubota, A. S. Jenkins, M. Romera, K. Yakushiji, A. Fukushima, J. Grollier, S. Yuasa, and V. Cros, Nat. Commun. **8**, 15825 (2017).

[36] R. Lehndorff, D. E. Bürgler, S. Gliga, R. Hertel, P. Grünberg, C. M. Schneider, and Z. Celinski, Phys. Rev. B **80**, 054412 (2009).

[37] S. Urazhdin, P. Tabor, V. Tiberkevich, and A. Slavin, Phys. Rev. Lett. **105**, 104101 (2010).

[38] V. S. Tiberkevich, A. N. Slavin, and J.-V. Kim, Phys. Rev. B **78**, 092401 (2008).

[39] K. V. Thadani, G. Finocchio, Z.-P. Li, O. Ozatay, J. C. Sankey, I. N. Krivorotov, Y.-T. Cui, R. A. Buhrman, and D. C. Ralph, Phys. Rev. B **78**, 024409 (2008).

[40] T. Valet and A. Fert, Phys. Rev. B **48**, 7099 (1993).

[41] J. S. Moodera and G. Mathon, J. Magn. Magn. Mater. **200**, 248 (1999).

[42] D. Houssameddine, U. Ebels, B. Delaët, B. Rodmacq, I. Firastrau, F. Ponthenier, M. Brunet, C. Thirion, J.-P. Michel, L. Prejbeanu-Buda, M.-C. Cyrille, O. Redon, and B. Dieny, Nat. Mater. **6**, 447 (2007).

[43] Y. Sun, H. Chang, M. Kabatek, Y.-Y. Song, Z. Wang, M. Jantz, W. Schneider, M. Wu, E. Montoya, B. Kardasz, B. Heinrich, S. G. E. te Velthuis, H. Schultheiss, and A. Hoffmann, Phys. Rev. Lett. **111**, 106601 (2013).

[44] M. J. Donahue and D. G. Porter, *OOMMF User's Guide, Version 1.0*, Interagency Report No. NISTIR 6376 (National Institute of Standards and Technology, Gaithersburg, MD, 1999).

[45] J. Guckenheimer, IEEE Trans. Circuits Syst. **27**, 983 (1980).

[46] Z. Z. Sun, S. Yin, X. R. Wang, J. P. Cao, Y. P. Wang, and Y. Q. Wang, Appl. Phys. Lett. **87**, 182110 (2005).

[47] R. Rand and P. Holmes, Int. J. Non-Linear Mech. **15**, 387 (1980).

[48] S. Wirkus and R. Rand, Nonlinear Dyn. **30**, 205 (2002).